Scripta Materialia 156 (2018) 64–69

Contents lists available at ScienceDirect

Scripta Materialia

journal homepage: www.elsevier.com/locate/scriptamat

Regular Article

Creation and modulation of conductivity in laser-irradiated $SrTiO_3$ single crystals

Z.T. Zhang, H. Yan, S.H. Wang, L.X. Ren, C.L. Chen, K.X. Jin *

Shaanxi Key Laboratory of Condensed Matter Structures and Properties, School of Natural and Applied Sciences, Northwestern Polytechnical University, Xi'an 710072, China

ARTICLE INFO

Article history:
Received 4 April 2018
Received in revised form 4 June 2018
Accepted 19 June 2018
Available online xxxx

Keywords:
Laser treatment
Oxides
Transmission electron microscopy
Surface
Transport properties

ABSTRACT

We realize a controllable metallic behavior on stoichiometric (100) $SrTiO_3$ single crystals via KrF laser irradiation, which strongly depends on vacuum and laser energy density. Moreover, this metallic conduction is caused by oxygen deficiency and can be manipulated by light illumination and electrostatic gating field. The laser-irradiated $SrTiO_3$ shows sensitive persistent photoresponse with a relative change in the resistance of about 45% at 20 K for a 360 nm light. In addition, the conduction can also be modulated to a lower (higher) state by a positive (negative) backgate. Our results highlight the possibility of tuning the electrical properties of oxides.

Transition-metal oxides with perovskite structure are a captivating family of materials, having rich phase diagrams and intriguing physical properties due to the interactions between multiple degrees of freedom. This allows us to design the devices with novel functionalities and advanced technologies in extensive fields [1–4]. Thereinto, $SrTiO_3$ (STO) single crystal is one of the most important and potentially useful oxides, exhibiting an indirect bandgap of ~3.2 eV and a cubic structure (Pm3m) at room temperature [5]. Meanwhile, it has many fascinating characteristics, including colossal magnetoresistance, ferroelectricity, quantum paraelectricity, superconductivity and two-dimensional electron gas (2DEG) [6–11].

In particular, manipulating conducting properties of STO single crystals is important for electronic and optoelectronic applications of oxides. Generally, the conducting STO crystals can be produced through various ways, including chemical doping, high-temperature annealing, noble-ion bombardment, H adsorption, electron-beam evaporation and field effect [12–21]. As a completely distinct route mentioned above, laser irradiation is an easily controllable and versatile method, having significant implications in surface modification, laser-based chemical analysis, and laser damage [22–24]. Recently, defect-induced ferromagnetism has been reported in STO by laser irradiation [23–25]. Meanwhile, considering the band gap and a transparent absorption in the ultraviolet region of <390 nm, the photoresistivity, photoluminescence and relaxation also have been systematically studied in bare and annealing STO systems [26–29]. More importantly, the emergent 2DEG has been observed at the bare STO only using angle-resolved photoemission spectroscopy [30]. We consider that the generation of conductivity is closely related with vacuum and laser energy density, and thus the influencing mechanism of two factors needs to be deeply revealed. Besides, the systematic studies on the real electron transport and its intrinsic mechanism are insufficient. In the work, we realize a controllable metallic behavior on stoichiometric (100) STO single crystals by laser irradiation and investigate the dependence of transport on vacuum and laser energy density. Furthermore, manipulating the transport of irradiated STO single crystals through optical and electrostatic modulation has been studied by using the metallic layer as electrodes.

Commercially available $5 \times 5 \times 0.5$ mm^3 stoichiometric (100) STO single crystals were used. Samples were irradiated for 20 s at room temperature by a KrF excimer laser (Lambda Physik) with a wavelength of 248 nm. The repetition rate was 1 Hz. The energy density of laser was varied from 350 to 650 mJ/cm^2 at a fixed oxygen pressure 5×10^{-4} Pa. In addition, the samples were also irradiated in the oxygen pressure of ~5×10^{-4}, 5×10^{-2}, 5 Pa and 1 atm at a constant energy density of 500 mJ/cm^2. Hall coefficient measurements were performed by the Van der Pauw method. The atomic force microscopy (AFM) and field emission scanning electron microscopy (SEM) were used to characterize surface morphologies of the samples. High-resolution transmission electron microscopy (HRTEM) images and electron diffraction (ED) images were collected by Tecnai G2F20S-TWIN. Electrical contacts with a spacing of 2 mm were made using Al wire bonding. The sheet resistance was measured in the Van der Pauw geometry. To identify the oxidation states of various elements of the STO before and after laser irradiation, X-ray photoelectron spectroscopy (XPS) was performed by using a Kratos Axis Ultra DLD spectrometer equipped with an Al Kα

* Corresponding author.
E-mail address: jinkx@nwpu.edu.cn (K.X. Jin).

https://doi.org/10.1016/j.scriptamat.2018.06.038
1359-6462/

monochromatic X-ray source. For optical measurements, samples were illuminated using the light with different wavelengths of 360, 473 and 650 nm. The power density was about 3 W/cm^2. Electrical field was applied to STO through an Ag electrode underneath STO and the STO surface was grounded. The direction from substrate to surface was defined as positive. The applied voltage for resistance measurements was 1 V. Under the gate voltage of 100 V, the leakage current was 1 nA.

Temperature dependence of the sheet resistance of STO single crystals irradiated under different partial pressures at a constant energy density of 500 mJ/cm^2 is shown in Fig. 1a. The samples irradiated at 5, 5×10^{-2} and 5×10^{-4} Pa display a metallic behavior, whereas the sample irradiated in air shows an insulating conduction. More strikingly, the sheet resistance monotonically decreases with decreasing the partial pressure over the entire temperature range. In addition, extremely low resistance is obtained when the sample is irradiated at 5×10^{-4} Pa. These results indicate that the conduction is correlated with the oxygen vacancy induced by laser irradiation. More oxygen vacancies are created at a lower oxygen pressure and result in a lower resistance. Fig. 1b shows the sheet resistances of irradiated STO at different energy densities as a function of temperature. The metallic behavior remains invariant at different laser energy densities. Nevertheless, the sheet resistance decreases first and then is followed by an increase with increasing the energy densities. This feature suggests that the oxygen vacancies become already saturated at larger energy density and amounts of local disorder induced by laser irradiation take the major responsibility for the increasing resistance. For the 425 mJ/cm^2 laser-irradiated STO at 5×10^{-4} Pa, the sheet resistance reaches a minimum value of 23 Ω/sq. at 20 K. Sheet carrier density and mobility are 1.0×10^{16} cm^{-2} and 27.4 cm^2 V^{-1} s^{-1} at 20 K, respectively. Overall, the vacuum plays a dominant role for the creation of conductivity and the energy density is followed. Moreover, the samples irradiated at the partial pressure of 5 and 5×10^{-2} Pa exhibit a typical metal-insulator transition at 239 and 241 K, respectively. The transition temperatures increase as decreasing oxygen partial pressure as shown in Fig. 1a. For the samples irradiated at the 575 and 650 mJ/cm^2 energy densities, the metal-insulator transition also is observed as shown in Fig. 1b. The transition temperatures increase as the laser energy decreases and finally the metal-insulator transition diminishes when the energy density is below 575 mJ/cm^2.

To explore the structural variations and morphology at the surface and cross-section, we select the sample irradiated at 425 mJ/cm^2 and 5×10^{-4} Pa. Typical AFM, SEM and TEM images of the sample are shown in Fig. 2. Obviously, many square areas appear on the surface as shown in Fig. 2a. The root-mean-square roughness is about 30 nm after laser irradiation. The formation of square areas might be caused by the reconstruction of STO surface after melting by the heating effect of intense laser. In addition, some microdefects are also observed, such as microcracks, as shown in Fig. 2b. The width of microcrack is about 50 nm. Atomic content of Ti and Sr in the batch electron spectra is nearly equivalent and the line scanning spectra is stable (see Fig. A1 of the supplemental materials). These results suggest that the relative content of Ti and Sr keeps invariable for the irradiated STO. In Fig. 2c, the cross-section HRTEM image presents a clear stratification, indicating that laser irradiation has a significant impact on the interior of sample. Fig. 2d and e show the HRTEM images of green and yellow zones marked in Fig. 2c, respectively. From Fig. 2d, we can see the breaking of dot matrix structure, indicating the occurrence of defective phase with a thickness of ~77 nm. Fig. 2e suggests that the initial cubic structure is thoroughly destroyed and an amorphous phase with a depth of ~55 nm is formed. The ED patterns in Fig. 2f and g from the point 'A' and 'B', respectively, present a clear dot matrix. In Fig. 2h, the ED pattern of point 'C' shows a halo-pattern, demonstrating the presence of amorphous phase. Basically, two mechanisms for laser irradiation of materials have been suggested: chemical bonds are broken due to the high density of electronic excitations caused by the absorption of photons; and atoms are emitted due to local thermal melting of the surface caused by intense laser irradiation. Both the mechanisms can lead to the melting and reconstruction on the surface of STO. And the initial cubic perovskite structure is damaged and changed into an amorphous state. Obviously, the defective layer results in the metallic behavior because the amorphous layer usually is insulating [31].

Furthermore, surface XPS analysis of samples is carried out to determine the elements and valence in laser-irradiated STO. As we know, the XPS technique is very surface sensitive. Therefore, for detecting the characteristics of conductive layer, the samples were in situ cleaned by low energy (1 keV) Ar^+ ion bombardment in the vacuum chamber before the XPS measurement. Fig. 3 shows the core level lines, O 1 s, Ti 2p and Sr 3d, for the pristine and laser-irradiated STO. The positions of all the lines have been calibrated according to the natural C1s spectra standard. Figs. 3a-c display the core level spectra of the irradiated samples at different partial pressures. The core level spectra of samples irradiated at different energy densities are presented in Figs. 3d-f. The Ti and Sr spectra exhibit two contributions, Ti2p3/2, Ti2p1/2, Sr3d3/2, and Sr3d5/2, respectively, which are ascribed to the spin-orbit split components. It can be seen that the line shapes, full width at half maximum and peak intensities are strongly modified after laser irradiation, indicating different chemical environments. And the peak positions shift distinctly, except for Ti 2p peaks. These significant changes of all spectra are nearly similar. In Fig. 3a and d, the splitting of O 1 s spectrum has been observed [32]. The lower binding energy component is

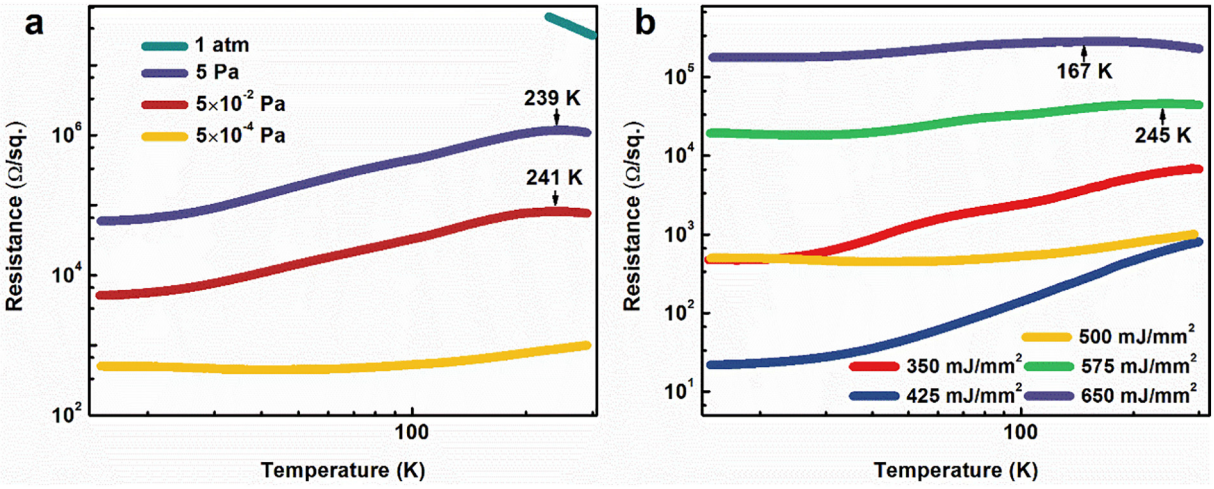

Fig. 1. a) Temperature dependence of the sheet resistance in air and the partial pressure of ~5, 5×10^{-2} and 5×10^{-4} Pa at the laser energy density of 500 mJ/cm^2. b. The sheet resistance of irradiated STO as a function of temperature at different energy densities in the partial pressure of 5×10^{-4} Pa.